Analytical Study of Momentum-Based Acceleration Methods in Paradigmatic High-Dimensional Non-Convex Problems

Stefano Sarao Mannelli
Department of Experimental Psychology
University of Oxford
Oxford, United Kingdom
`stefano.saraomannelli@psy.ox.ac.uk`

Pierfrancesco Urbani
Université Paris-Saclay, CNRS, CEA
Institut de physique théorique
Gif-sur-Yvette, France
`pierfrancesco.urbani@ipht.fr`

Abstract

The optimization step in many machine learning problems rarely relies on vanilla gradient descent but it is common practice to use momentum-based accelerated methods. Despite these algorithms being widely applied to arbitrary loss functions, their behaviour in generically non-convex, high dimensional landscapes is poorly understood. In this work, we use dynamical mean field theory techniques to describe analytically the average dynamics of these methods in a prototypical non-convex model: the (spiked) matrix-tensor model. We derive a closed set of equations that describe the behaviour of heavy-ball momentum and Nesterov acceleration in the infinite dimensional limit. By numerical integration of these equations, we observe that these methods speed up the dynamics but do not improve the algorithmic threshold with respect to gradient descent in the spiked model.

1 Introduction

In many computer science applications one of the critical steps is the minimization of a cost function. Apart from very few exceptions, the simplest way to approach the problem is by running local algorithms that move down in the cost landscape and hopefully approach a minimum at a small cost. The simplest algorithm of this kind is gradient descent, that has been used since the XIX century to address optimization problems [1]. Later on, faster and more stable algorithms have been developed: second order methods [2, 3, 4, 5, 6, 7] where information from the Hessian is used to adapt the descent to the local geometry of the cost landscape, and first order methods based on momentum [8, 9, 10, 11, 12] that introduce inertia in the algorithm and provably speed up convergence in a variety of convex problems. In the era of deep-learning and large datasets, the research has pushed towards memory efficient algorithms, in particular stochastic gradient descent that trades off computational and statistical efficiency [13, 14], and momentum-based methods are very used in practice [15]. Which algorithm is the best in practice seems not to have a simple answer and there are instances where a class of algorithms outperforms the other and vice-versa [16]. Most of the theoretical literature on momentum-based methods concerns convex problems [17, 18, 19, 20, 21] and, despite these methods have been successfully applied to a variety of problems, only recently high dimensional non-convex settings have been considered [22, 23, 24]. Furthermore, with few exceptions [25], the majority of these studies focus on *worst-case* analysis while empirically one could also be interested in the behaviour of such algorithms on typical instances of the optimization problem, formulated in terms of a generative model extracted from a probability distribution.

The main contribution of this paper is the analytical description of the average evolution of momentum-based methods in two simple non-convex, high-dimensional, optimization problems. First we consider the mixed p-spin model [26, 27], a paradigmatic random high-dimensional optimization problem.

Furthermore we consider its spiked version, the spiked matrix-tensor [28, 29] which is a prototype high-dimensional non-convex inference problem in which one wants to recover a signal hidden in the landscape. The second main result of the paper is the characterization of the algorithmic threshold for accelerated-methods in the inference setting and the finding that this seems to coincide with the threshold for gradient descent.

The definition of the model and the algorithms used are reported in section 2. In section 3 and 4 we use dynamical mean field theory [30, 31, 32] to derive a set of equations that describes the average behaviour of these algorithms starting from random initialization in the high dimensional limit and in a fully non-convex setting.

We apply our equations to the spiked matrix-tensor model [29, 33, 34], which displays a similar phenomenology as the one described in [24, 35] for the phase retrieval problem: all algorithms have two dynamical regimes. First, they navigate in the non-convex landscape and, second, if the signal to noise ratio is strong enough, the dynamics eventually enters in the basin of attraction of the signal and rapidly reaches the bottom of the cost function. We use the derived state evolution of the algorithms to determine their algorithmic threshold for signal recovery.

Finally, in Sec. 5 we show that in the analysed models, momentum-based methods only have an advantage in terms of speed but they do not outperform vanilla gradient descent in terms of the algorithmic recovery threshold.

2 Model definition

We consider two paradigmatic non-convex models: the mixed p-spin model [32, 36], and the spiked matrix-tensor model [28, 29]. Given a tensor $\boldsymbol{T} \in (\mathbb{R}^N)^{\otimes p}$ and a matrix $\boldsymbol{Y} \in \mathbb{R}^{N \times N}$, the goal is to find a common low-rank representation $\boldsymbol{x}$ that minimizes the loss

$$\mathcal{L} = -\frac{1}{\Delta_p} \sqrt{\frac{(p-1)!}{N^{p-1}}} \sum_{i_1,\ldots,i_p=1}^{N} T_{i_1,\ldots,i_p} x_{i_1} \ldots x_{i_p} - \frac{1}{\Delta_2} \frac{1}{\sqrt{N}} \sum_{i,j=1}^{N} Y_{ij} x_i x_j, \tag{1}$$

with $\boldsymbol{x}$ in the N-dimensional sphere of radius $\sqrt{N}$. The two problems differ by the definition of the variables $\boldsymbol{T}$ and $\boldsymbol{Y}$. Call $\boldsymbol{\xi}^{(p)}$ and $\boldsymbol{\xi}^{(2)}$ order p tensor and a matrix having i.i.d. Gaussian elements, with zero mean and variances Δ_p and Δ_2 respectively. In the mixed p-spin model, tensor and matrix are completely random $\boldsymbol{T} = \boldsymbol{\xi}^{(p)}$ and $\boldsymbol{Y} = \boldsymbol{\xi}^{(2)}$. While in the spiked matrix-tensor model there is a low-rank representation given by $\boldsymbol{x}^* \in \mathcal{S}^{N-1}(\sqrt{N})$ embedded in the problem as follows:

$$T_{i_1\ldots i_p} = \sqrt{\frac{(p-1)!}{N^{p-1}}} x_{i_1}^* \ldots x_{i_p}^* + \xi_{i_1\ldots i_p}^{(p)}, \qquad Y_{ij} = \frac{x_i^* x_j^*}{\sqrt{N}} + \xi_{ij}^{(2)}. \tag{2}$$

These problems have been studied both in physics, and computer science. In the physics literature, research has focused on the relationship of gradient descent and Langevin dynamics and the corresponding topology of the complex landscape [32, 37, 38, 36, 39, 27, 40]. The state evolution of the gradient descent dynamics for the mixed spiked matrix-tensor model has been studied only more recently [33, 34]. All these works considered simple gradient descent dynamics and its noisy (Langevin) dressing.

In this work we focus on accelerated methods and provide an analytical characterization of the average performance of these algorithms for the models introduced above. In order to simplify the analysis we relax the hard constraint on the norm of the vector $\boldsymbol{x}$ and consider $\boldsymbol{x} \in \mathbb{R}^N$ while adding a penalty term to $\mathcal{L}$ to enforce a soft constraint $\frac{\mu}{4N}\left(\sum_i x_i^2 - N\right)^2$, so that the total cost function is $\mathcal{H} = \mathcal{L} + \frac{\mu}{4N}\left(\sum_i x_i^2 - N\right)^2$. Using the techniques described in detail in the next section we write the state evolution for the following algorithms:

- **Nesterov acceleration** [9] starting from $\boldsymbol{y}[0] = \boldsymbol{x}[0] \in \mathbb{S}^{N-1}\left(\sqrt{N}\right)$

$$\boldsymbol{x}[t+1] = \boldsymbol{y}[t] - \alpha \nabla \mathcal{H}(\boldsymbol{y}[t]), \tag{3}$$

$$\boldsymbol{y}[t+1] = \boldsymbol{x}[t+1] + \frac{t}{t+3}\left(\boldsymbol{x}[t+1] - \boldsymbol{x}[t]\right). \tag{4}$$

given α the learning rate of the algorithm.

- **Polyak's or heavy ball momentum** (HB) [8] starting from $\boldsymbol{y}[0] = \boldsymbol{0}$ and $\boldsymbol{x}[0] \in \mathbb{S}^{N-1}\left(\sqrt{N}\right)$, given the parameters α, β

$$\boldsymbol{y}[t+1] = \beta\boldsymbol{y}[t] + \nabla\mathcal{H}(\boldsymbol{x}[t]), \tag{5}$$
$$\boldsymbol{x}[t+1] = \boldsymbol{x}[t] - \alpha\boldsymbol{y}[t+1]; \tag{6}$$

- **gradient descent** (GD) starting from $\boldsymbol{x}[0] \in \mathbb{S}^{N-1}\left(\sqrt{N}\right)$

$$\boldsymbol{x}[t+1] = \boldsymbol{x}[t] - \alpha\nabla\mathcal{H}(\boldsymbol{x}[t]). \tag{7}$$

This case has been considered in [27, 33] with the constraint $\sum_i x_i^2 = N$. The generalization to the present case in which constraint is soft is a straightforward small extension of these previous works.

We will not compare the performance of these accelerated gradient methods to algorithms of different nature (such as for example message passing ones) in the same settings. Our goal will be the derivation of a set of dynamical equations describing the average evolution of such algorithms in the high dimensional limit $N \to \infty$.
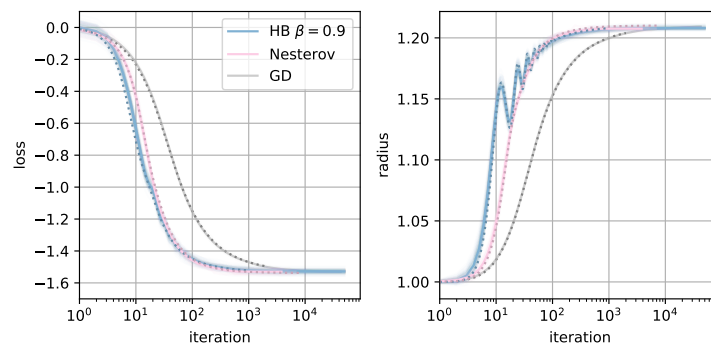
3 Dynamical mean field theory

Figure 1: **Simulation and DMFT comparison in mixed p-spin model.** The simulations in the figures have parameters $p = 3$, $\Delta_3 = 2/p$, $\Delta_2 = 1$, ridge parameter $\mu = 10$ and input dimension $N = 1024$. In all our simulations we use the dilution technique [41, 42] to reduce the computational cost. We consider: Nesterov acceleration in pink; heavy ball momentum in blue with $\alpha = 0.01$ and $\beta = 0.9$; and gradient descent in grey. We run 100 simulations (in transparency) and draw the average. The parameters for heavy ball are the best parameters found in our simulations, see also Fig. 2 for a comparison. The results from the DMFT equations are drawn with dotted lines.

We use dynamical mean field theory (DMFT) techniques to derive a set of equation describing the evolution of the algorithms in the high-dimensional limit. The method has its origin in statistical physics and can be applied to the study of Langevin dynamics of disordered systems [30, 31, 43]. More recently it was proved to be rigorous in the case of the mixed p-spin model [44, 45]. The application to the inference version of the optimization problem is in [29, 33]. The same techniques have also been applied to study the stochastic gradient descent dynamics in single layer networks [46] and in the analysis of recurrent neural networks [47, 48, 49].

The derivation presented in the rest of the section is heuristic and, as such, it is not fully rigorous. Making our results rigorous would be an extension of the works [44, 45] where path-integral methods are used to prove a large deviation principle for the infinite-dimensional limit. Our non-rigorous results are checked against extensive numerical simulations.

The idea behind DMFT is that, if the input dimension N is sufficiently large, one can obtain a description of the dynamics in terms of the typical evolution of a representative entry of the vector $\boldsymbol{x}$ (and vector $\boldsymbol{y}$ when it applies). The representative element evolves according to a non-Markovian

stochastic process whose memory term and noise source encode, in a self-consistent way, the interaction with all the other components of vector $\boldsymbol{x}$ (and $\boldsymbol{y}$). The memory terms as well as the statistical properties of the noise are described by dynamical order parameters which, in the present model, are given by the dynamical two-time correlation and response functions.

In this first step of the analysis we obtain an effective dynamics for a representative entry x_i (and y_i). The next step consists in using such equations to compute self-consistently the properties of the corresponding stochastic processes, namely the memory kernel and the statistical correlation of the noise. In Fig. 1 we anticipate the results by comparing numerical simulations with the integration of the DMFT equations for the different algorithms: on the left we observe the evolution of the loss, on the right we observe the evolution of the radius of the vector $\boldsymbol{x}$, defined as the L_2 norm of the vector $||\boldsymbol{x}||_2$. We find a good agreement between the DMFT state evolution and the numerical simulations.

We compare Nesterov acceleration with the heavy ball momentum in the mixed p-spin model Fig. 1, and in the spiked model Fig. 3. Nesterov acceleration allows for a fast convergence to the asymptotic energy without need of parameter tuning. In Fig. 2 we compare the numerical simulations for the HB algorithm and the DMFT description of the corresponding massive momentum version for several control parameters.

DMFT equations

In the following we describe the resulting DMFT equations for the correlation and response functions. The details of their derivation for the case of the Nesterov acceleration are provided in the following section, while we leave the other cases to the supplementary material (SM). The dynamical order parameters appearing in the DMFT equations are one-time or two-time correlations, e.g. $C_{xy}[t, t'] = \sum_i x_i[t]y_i[t']/N$, and response to instantaneous perturbation of the dynamics, e.g. $R_x[t, t'] = \left(\sum_i \delta x_i[t]/\delta H_i[t'] \right)/N$ by a local field $\boldsymbol{H}[t'] \in \mathbb{R}^N$ where the symbol δ denotes the functional derivative. In this section we show only the equations for the mixed p-spin model and we discuss the difference and the derivation of the equations for the spiked tensor in the SM.

From the order parameters we can evaluate useful quantities that describe the evolution of the algorithms. In particular in Figs. 1,2,3 we show the loss, the radius, and the overlap with the solution in the spiked case (Fig. 3):

- Average loss

$$\mathcal{L}[t] = -\frac{\alpha}{\Delta_p C_x[t,t]^{\frac{p}{2}}} \sum_{t''=0}^{t} R_x[t,t']C_x[t,t']^{p-1} - \frac{\alpha}{\Delta_2 C_x[t,t]} \sum_{t''=0}^{t} R_x[t,t']C_x[t,t']; \quad (8)$$

- Radius $\sqrt{C_x[t,t]}$;

- Define $m_x[t] = \frac{1}{N}\sum_i x_i[t]x_i^*$ an additional order parameter for the spiked matrix-tensor model (more details are given in the SM), the overlap with ground truth is

$$\frac{\boldsymbol{x}[t] \cdot \boldsymbol{x}^*}{||\boldsymbol{x}||} = \frac{m_x[t]}{\sqrt{C_x[t,t]}}$$

Nesterov acceleration. It has been shown that this algorithm has a quadratic convergence rate to the minimum in convex optimization problems under Lipschitz loss functions [9, 50], thus it outperforms standard gradient descent whose convergence is linear in the number of iterations. The analysis of the algorithm is described by the flow of the following dynamical correlation functions

$$C_x[t, t'] = \frac{1}{N}\sum_i x_i[t]x_i[t'], \quad (9)$$

$$C_y[t, t'] = \frac{1}{N}\sum_i y_i[t]y_i[t'], \quad (10)$$

$$C_{xy}[t, t'] = \frac{1}{N}\sum_i x_i[t]y_i[t'], \quad (11)$$

4

$$R_x[t, t'] = \frac{1}{N} \sum_i \frac{\delta x_i[t]}{\delta H_i[t']}, \tag{12}$$

$$R_y[t, t'] = \frac{1}{N} \sum_i \frac{\delta y_i[t]}{\delta H_i[t']}. \tag{13}$$

The dynamical equations are obtained following the procedure detailed in section 4. Call $Q(x) = x^2/(2\Delta_2) + x^p/(p\Delta_p)$,

$$C_x[t+1, t'] = C_{xy}[t, t'] - \alpha\mu \left(C_y[t, t] - 1 \right) C_y[t, t'] + \alpha^2 \sum_{t''=0}^{t'} R_x[t', t'']Q'\left(C_y[t, t'']\right) +$$
$$+ \alpha^2 \sum_{t''=0}^{t} R_y[t, t'']Q''\left(C_y[t, t'']\right) C_{xy}[t', t'']; \tag{14}$$

$$C_{xy}[t+1, t'] = C_y[t, t'] - \alpha\mu \left(C_y[t, t] - 1 \right) C_{xy}[t, t'] + \alpha^2 \sum_{t''=0}^{t'} R_y[t', t'']Q'\left(C_y[t, t'']\right) +$$
$$+ \alpha^2 \sum_{t''=0}^{t} R_y[t, t'']Q''\left(C_y[t, t'']\right) C_y[t', t'']; \tag{15}$$

$$C_{xy}[t', t+1] = \frac{2t+3}{t+3}C_x[t+1, t'] - \frac{t}{t+3}C_x[t, t']; \tag{16}$$

$$C_y[t', t+1] = \frac{2t+3}{t+3}C_{xy}[t+1, t'] - \frac{t}{t+3}C_{xy}[t, t']; \tag{17}$$

$$R_x[t+1, t'] = R_y[t, t'] + \delta_{t,t'} - \alpha\mu \left(C_y[t, t] - 1 \right) R_y[t, t']$$
$$+ \alpha^2 \sum_{t''=t'}^{t} R_y[t, t'']R_y[t'', t']Q''\left(C_y[t, t'']\right); \tag{18}$$

$$R_y[t', t+1] = \frac{2t+3}{t+3}R_x[t+1, t'] - \frac{t}{t+3}R_x[t, t']. \tag{19}$$

The initial conditions are: $C_x[0, 0] = 1$, $C_y[0, 0] = 1$, $C_{xy}[0, 0] = 1$, $R_x[t+1, t] = 1$, $R_y[t+1, t] = \frac{2t+3}{t+3}$.

The equations show a discretized version of the typical structure of DMFT equations. We can observe: terms immediately ascribable to the dynamical equations (3,4) and summations whose interpretation is less trivial without looking into the derivation. They represent memory kernels that take into account linear response theory for small perturbations to the dynamics (e.g. the last term of Eq. (14)) and a noise whose statistical properties encode the effect of all the degrees of freedom on a representative one (e.g. the second last term of Eq. (14)).

Heavy ball momentum. The DMFT equations are obtained analogously to previous ones,

$$C_y[t+1, t'] = \beta C_y[t, t'] + \mu \left(C_x[t, t] - 1 \right) C_{xy}[t, t'] + \alpha \sum_{t''=0}^{t'} R_y[t', t'']Q'\left(C_x[t, t'']\right)$$
$$+ \alpha \sum_{t''=0}^{t} R_x[t, t'']Q''\left(C_x[t, t'']\right) C_{xy}[t'', t']; \tag{20}$$

$$C_{xy}[t', t+1] = \beta C_{xy}[t', t] + \mu \left(C_x[t, t] - 1 \right) C_x[t, t'] + \alpha \sum_{t''=0}^{t'} R_x[t', t'']Q'\left(C_x[t, t'']\right)$$
$$+ \alpha \sum_{t''=0}^{t} R_x[t, t'']Q''\left(C_x[t, t'']\right) C_x[t', t'']; \tag{21}$$

$$C_{xy}[t+1, t'] = C_{xy}[t, t'] - \alpha C_y[t+1, t']; \tag{22}$$

$$C_x[t+1, t'] = C_x[t, t'] - \alpha C_{xy}[t', t+1]; \tag{23}$$

5

$$R_y[t+1,t'] = \beta R_y[t,t'] + \frac{1}{\alpha}\delta_{t,t'} + \mu\left(C_x[t,t]-1\right)R_x[t,t']$$

$$+ \alpha \sum_{t''=0}^{t} R_x[t,t'']R_x[t'',t']Q''\left(C_x[t,t'']\right); \tag{24}$$

$$R_x[t+1,t'] = R_x[t,t'] - \alpha R_y[t+1,t']. \tag{25}$$

with initial conditions: $C_x[0,0]=1$, $C_y[0,0]=0$, $C_{xy}[0,0]=0$, $R_y[t+1,t]=1/\alpha$, $R_x[t+1,t]=-1$. Fig. 2 shows the consistency of theory and simulations.

Mappings between discrete update equation and continuous flow for both heavy ball momentum and Nesterov acceleration have been proposed in the literature. In the SM we considered the work [51] that maps HB to second order ODEs in some regimes of α and β. This mapping establishes the equivalence of the algorithm to the physics problem of a massive particle moving under the action of a potential. This problem has been studied in [52] but the result is limited to the fully under-damped regime where there is no first order derivative term, corresponding therefore to a dynamics that is fully inertial and which never stops due to energy conservation. In the SM we obtain the dynamical equations for arbitrary damping regimes, and we recover the equivalence established in [51] comparing the results from the two DMFTs formulations.

Gradient descent. A simple way to obtain the gradient descent DMFT is by taking the limit $m \to 0$ in the DMFT of the massive momentum description of HB. We get

$$C_x[t+1,t'] = C_x[t,t'] - \alpha\mu\left(C_x[t,t]-1\right)C_x[t,t'] + \alpha^2\sum_{t''=0}^{t'}R_x[t',t'']Q'\left(C_x[t,t'']\right)$$

$$+ \alpha^2\sum_{t''=0}^{t}R_x[t,t'']Q''\left(C_x[t,t'']\right)C_x[t',t'']; \tag{26}$$

$$R_x[t+1,t'] = R_x[t,t'] + \delta_{t,t'} + \alpha^2\sum_{t''=0}^{t}R_x[t,t'']R_x[t'',t']Q''\left(C_x[t,t'']\right)$$

$$- \alpha\mu\left(C_x[t,t]-1\right)R_x[t,t']. \tag{27}$$

with initial conditions: $C_x[0,0]=1$, and $R_x[t+1,t]=1$. Apart from the μ-dependent term, these equations are a particular case of the ones that appear in [36, 37] and we point to these previous references for details.
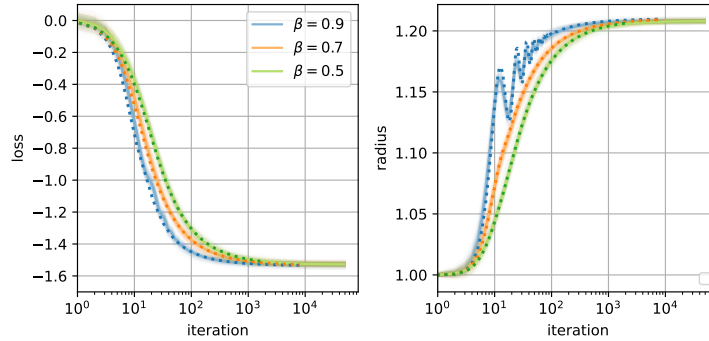

Figure 2: **DMFT for HB.** Simulations of HB momentum in the mixed p-spin model with $p = 3$, $\Delta_3 = 2/p$, $\Delta_2 = 1$, ridge parameter $\mu = 10$ and input dimension $N = 1024$. The parameters are $\alpha = 0.01$ for all the simulations and $\beta \in \{0.5, 0.7, 0.9\}$. We use solid lines to represent the result from the simulation, the dotted lines for the DMFT of HB.
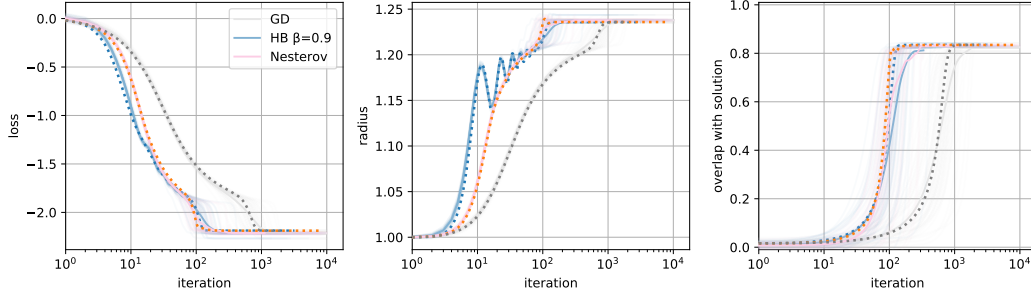
Figure 3: **DMFT in the spiked matrix-tensor model.** Performance of heavy ball and Nesterov in the spiked matrix-tensor model with $p = 3$, $1/\Delta_2 = 2.7$, $\Delta_3 = 1.0$, and $\mu = 10$. The parameters in the simulations are: $\alpha = 0.01$ and $\beta = 0.9$ for HB. The different solid lines correspond to simulations with input dimension $N = 8192$, while the dotted lines are obtained from the DMFT that, by definition, is in the infinite dimension limit. In the spiked version of the model the finite size effects are stronger and larger simulation sizes are needed.

4 Derivation of DMFT for Nesterov acceleration

The approach for the DMFT proposed in this section is based on the dynamical cavity method [43]. Consider the problem having dimension $N + 1$ and denote the additional entry of the vectors $\boldsymbol{x}$ and $\boldsymbol{y}$ with the subscript 0, x_0 and y_0. The idea behind cavity method is to evaluate how this additional dimension changes the dynamics of all degrees of freedom. If the dimension is sufficiently large the dynamics is only slightly modified by the additional dimension, and the effect of the additional degree of freedom can be tracked in perturbation theory.

The framework described in this section might be extended to more other momentum-based algorithms (such as PID [11] and quasi-hyperbolic momentum [12]) with some minor adaptations. The steps to follow [43] can be summarised in:

- Writing the equation of motion isolating the contributions of an additional degree of freedom, leading to Eqs. (28-30;
- Treating the effect of the terms containing the new degree of freedom in perturbation theory, Eqs. (32-34);
- Identifying the order dynamical order parameters, namely dynamical correlation and response functions, Eqs. (37,38).

Consider the Nesterov update algorithm and isolate the effect of the additional degree of freedom

$$x_i[t + 1] = y_i[t] + \alpha \sum_{j \neq 0} J_{ij} y_j[t] + \alpha \sum_{(i,i_2,\ldots,i_p)} J_{i,i_2,\ldots,i_p} y_{i_2}[t] \ldots y_{i_p}[t] - \alpha \mu \left(\sum_{j \neq 0} \frac{y_j^2[t]}{N} - 1 \right) y_i[t] \tag{28}$$

$$+ \alpha \sum_{(i,0,i_3,\ldots,i_p)} J_{i,0,i_3,\ldots,i_p} y_0[t] y_{i_3}[t] \ldots y_{i_p}[t] + \alpha J_{i0} y_0[t] + \frac{\mu}{N} y_0^2[t] y_i[t], \tag{29}$$

$$y_i[t + 1] = x_i[t + 1] + \frac{t}{t + 3} \left(x_i[t + 1] - x_i[t] \right). \tag{30}$$

We identify the term in line (29) as a perturbation, denoted by $H_i[t]$. We will assume that the perturbation is sufficiently small and the effective dynamics is well approximated by a first order expansion around the original updates, so-called *linear response regime*. Therefore, the perturbed entries can be written as

$$x_i[t] \approx x_i^0 + \alpha \sum_{t''=0}^{t} \frac{\delta x_i[t]}{\delta H_i[t'']} H_i[t''], \qquad y_i[t] \approx y_i^0 + \alpha \sum_{t''=0}^{t} \frac{\delta y_i[t]}{\delta H_i[t'']} H_i[t'']. \tag{31}$$

7

The dynamics of the 0th degree of freedom to the leading order in the perturbation is

$$x_0[t+1] = y_0[t] - \alpha\mu\Big(\frac{1}{N}\sum_j y_j^2[t] - 1\Big)y_0[t] + \Xi[t] + \alpha^2 \sum_j J_{0j} \sum_{t''=0}^{t} \frac{\delta y_j[t]}{\delta H_j[t'']} H_j[t''] \quad (32)$$

$$+ \alpha^2 \sum_{(0,i_2,\dots,i_p)} J_{0,i_2,\dots,i_p} \Big(\sum_{t''=0}^{t} \frac{\delta y_{i_2}[t]}{\delta H_{i_2}[t'']} H_{i_2}[t''] y_{i_3}[t] \dots y_{i_p}[t] + \text{perm.} \Big) + \mathcal{O}\Big(\frac{1}{N}\Big), \quad (33)$$

$$y_i[t+1] = x_i[t+1] + \frac{t}{t+3}\left(x_i[t+1] - x_i[t]\right), \quad (34)$$

with $\Xi = \alpha \sum_j J_{0j} y_j[t] + \alpha \sum_{(0,i_2,\dots,i_p)} J_{0,i_2,\dots,i_p} y_{i_2}[t] \dots y_{i_p}[t]$ a Gaussian noise with moments:

$$\mathbb{E}[\Xi[t]] = 0,$$

$$\mathbb{E}[\Xi[t]\Xi[t']] = \frac{1}{\Delta_2}C_y[t,t'] + \frac{1}{\Delta_p}C_y^{p-1}[t,t'] = Q'\left(C_y[t,t']\right) \doteq \mathbb{K}[t,t'].$$

The terms in Eqs. (32,33) can be simplified. Consider the last term in Eq. (32): after substituting the H_i, $J_{0j}J_{0j}$ and $J_{0j}J_{(j,0,\dots,i_p)}$ can be approximated by their expected values with a difference that is subleading in $1/N$

$$\alpha^2 \sum_j J_{0j} \sum_{t''=0}^{t} \frac{\delta y_j[t]}{\delta H_j[t'']} J_{0j} y_0[t''] \approx \frac{\alpha^2}{\Delta_2 N} \sum_{t''=0}^{t} \frac{\delta y_j[t]}{\delta H_j[t'']} y_0[t''] = \frac{\alpha^2}{\Delta_2} \sum_{t''=0}^{t} R_y[t,t''] y_0[t''], \quad (35)$$

where the last equality follows from the definition of response function in y.
The same approximation is applied to Eq. (33), taking carefully into account the permutations, obtaining

$$\frac{\alpha^2(p-1)}{\Delta_p} \sum_{t''=0}^{t} R_y[t,t''] \left(C_y[t,t'']\right)^{p-2} y_0[t'']. \quad (36)$$

Finally, collecting all terms, the effective dynamics of the additional dimension is given by

$$x_0[t+1] = y_0[t] + \alpha\Xi[t] - \alpha\mu\left(C_y[t,t] - 1\right)y_0[t] + \alpha^2 \sum_{t''=0}^{t} R_y[t,t''] Q''\left(C_y[t,t'']\right) y_0[t'']; \quad (37)$$

$$y_0[t+1] = x_0[t+1] + \frac{t}{t+3}\left(x_0[t+1] - x_0[t]\right). \quad (38)$$

In order to derive the updates of the order parameters, we need the expected values of $\langle\Xi[t]x_0[t']\rangle$ and $\langle\Xi[t]y_0[t']\rangle$ with respect to the stochastic process. These are obtained using Girsanov theorem

$$\langle\Xi[t]x_0[t']\rangle = \alpha \sum_{t''} R_x[t',t''] Q'\left(C_y[t,t'']\right), \qquad \langle\Xi[t]y_0[t']\rangle = \alpha \sum_{t''} R_y[t',t''] Q'\left(C_y[t,t'']\right).$$

The final step consists in substituting the Eqs. (37,38) into the equations of the order parameters Eqs. (14-19). Then we identify the order parameters in the equations and use the results of Girsanov theorem to obtain the dynamical equations reported in section 3.

5 Algorithmic threshold

Finally we investigate the performance of accelerated methods in recovering a signal in a complex non-convex landscape. The dynamics of the gradient descent has been studied in the spiked matrix-tensor model in [33]. Using DMFT it was possible to compute the phase diagram for signal recovery in terms of the noise levels Δ_2 and Δ_p. This phase diagram was later confirmed theoretically [34].

Given the DMFT equations derived in the previous sections we can apply the analysis used in [33] to accelerated gradient methods. Given order of the tensor p and Δ_p, increasing Δ_2 the problem becomes harder and moves from the easy phase - where the signal can be partially recovered - to an algorithmically impossible phase - where the algorithm remains stuck at vanishingly small overlap
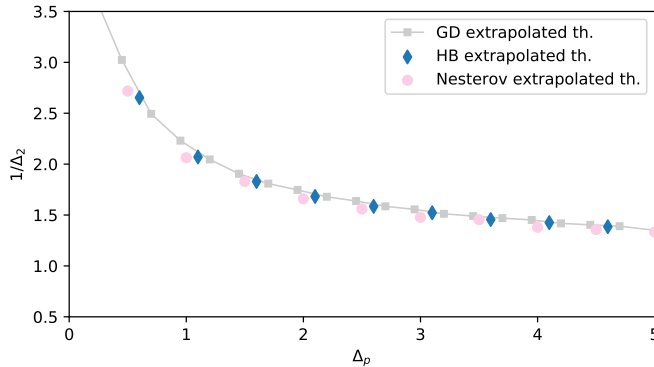
Figure 4: **Phase diagram of the spiked matrix-tensor model.** The horizontal and vertical axis represent the parameters of the model Δ_p and $1/\Delta_2$. We identify two regions in the diagram: where Nesterov, heavy ball and gradient descent algorithms lead to the hidden solution (upper region), and where they fail (lower region). The grey square connected by a solid line represents the threshold of gradient descent estimated numerically as detailed in the text. We use points to indicate the threshold extrapolated from the DMFT: pink circles for Nesterov acceleration and blue diamonds for heavy ball momentum with $\beta = 0.9$ and $\alpha = 0.01$.

with the signal. The goal of the analysis is to characterize the algorithmic threshold that separates the two phases. Using the DMFT we estimate the *relaxation time* – the time the accelerated methods need to find the signal. Since this time diverges approaching the algorithmic threshold, the fit of the divergence point gives an estimation of the threshold.

More precisely, for each value of Δ_p as the noise to signal ratio (Δ_2) increases the simulation time required to arrive close to the signal[1] increases like a power law $\sim a\, |\Delta_2 - \Delta_2^{al\cdot}(\Delta_p)|^{-\theta}$. The algorithmic threshold $\Delta_2^{al\cdot}(\Delta_p)$ is obtained by fitting the parameters of the power law $(a, \theta, \Delta_2^{al\cdot})$. In the SM we show an example of the extrapolation of a single point where many initial conditions $m_x(0)$ are considered in order to correctly characterize the limits $N \to \infty$ and $m_x(0) \to 0^+$. Finally the fits obtained for the three algorithms and for several Δ_p are shown in the phase diagram of Fig. 4 for $p = 3$. We observe that all the algorithms give very close thresholds. DMFT allows to obtain a good estimation of the threshold, free from finite size effects and stochastic fluctuations that are present in the direct estimation from the simulations.

Conclusions and broader impact

In this work we analysed momentum-accelerated methods in two paradigmatic high-dimensional non-convex problems: the mixed p-spin model and the spiked matrix-tensor model. Our analysis is based on dynamical mean field theory and provides a set of equations that characterize the average evolution of the dynamics. We have focused on Polyak's heavy ball and Nesterov acceleration, but the same techniques may be applied to more recent methods such as quasi-hyperbolic momentum [12] and proportional integral-derivative control algorithm [11].

Momentum-based methods are techniques commonly used in practice but poorly understood at the theoretical level. This work analysed the dynamics of momentum-based algorithms in a very controlled setting of a high-dimensional non-convex inference problem which allowed us to establish that accelerated methods have a recovery threshold which is – within the limits of numerical integration – the same of vanilla gradient descent.

Our analysis can be easily extended to 1-layer neural networks – combining our technical results with the techniques of [46] – and to simple inference problem seen from the learning point of view, such as the phase retrieval problem [53]. The same questions can also be analysed in the context of recurrent networks [48, 49] where DMFT approaches have already been applied to gradient-based methods.

---

[1]Since the best possible overlap for maximum a posteriori estimator m^{MAP} can be computed explicitly, "close" means the time that the algorithms takes to arrive at $0.9 m^{\mathrm{MAP}}$

Our study is theoretical in nature and we do not foresee any societal impact.

Acknowledgments

References

[1] Augustin Cauchy. Méthode générale pour la résolution des systemes d'équations simultanées. *Comp. Rend. Sci. Paris*, 25(1847):536–538, 1847.

[2] Kenneth Levenberg. A method for the solution of certain non-linear problems in least squares. *Quarterly of applied mathematics*, 2(2):164–168, 1944.

[3] Donald W Marquardt. An algorithm for least-squares estimation of nonlinear parameters. *Journal of the society for Industrial and Applied Mathematics*, 11(2):431–441, 1963.

[4] Charles G Broyden. The convergence of a class of double-rank minimization algorithms: 2. the new algorithm. *IMA journal of applied mathematics*, 6(3):222–231, 1970.

[5] Roger Fletcher. A new approach to variable metric algorithms. *The computer journal*, 13(3):317–322, 1970.

[6] Donald Goldfarb. A family of variable-metric methods derived by variational means. *Mathematics of computation*, 24(109):23–26, 1970.

[7] David F Shanno. Conditioning of quasi-newton methods for function minimization. *Mathematics of computation*, 24(111):647–656, 1970.

[8] Boris T Polyak. Some methods of speeding up the convergence of iteration methods. *USSR Computational Mathematics and Mathematical Physics*, 4(5):1–17, 1964.

[9] Yurii E Nesterov. A method for solving the convex programming problem with convergence rate o (1/k^ 2). In *Dokl. akad. nauk Sssr*, volume 269, pages 543–547, 1983.

[10] Saman Cyrus, Bin Hu, Bryan Van Scoy, and Laurent Lessard. A robust accelerated optimization algorithm for strongly convex functions. In *2018 Annual American Control Conference (ACC)*, pages 1376–1381. IEEE, 2018.

[11] Wangpeng An, Haoqian Wang, Qingyun Sun, Jun Xu, Qionghai Dai, and Lei Zhang. A pid controller approach for stochastic optimization of deep networks. In *Proceedings of the IEEE Conference on Computer Vision and Pattern Recognition*, pages 8522–8531, 2018.

[12] Jerry Ma and Denis Yarats. Quasi-hyperbolic momentum and adam for deep learning. In *7th International Conference on Learning Representations, ICLR 2019, New Orleans, LA, USA, May 6-9, 2019*. OpenReview.net, 2019.

[13] Herbert Robbins and Sutton Monro. A stochastic approximation method. *The annals of mathematical statistics*, pages 400–407, 1951.

[14] Ilya Sutskever, James Martens, George Dahl, and Geoffrey Hinton. On the importance of initialization and momentum in deep learning. In *International conference on machine learning*, pages 1139–1147. PMLR, 2013.

[15] Laurent Lessard, Benjamin Recht, and Andrew Packard. Analysis and design of optimization algorithms via integral quadratic constraints. *SIAM Journal on Optimization*, 26(1):57–95, 2016.

[16] Rahul Kidambi, Praneeth Netrapalli, Prateek Jain, and Sham Kakade. On the insufficiency of existing momentum schemes for stochastic optimization. In *2018 Information Theory and Applications Workshop (ITA)*, pages 1–9. IEEE, 2018.

[17] Euhanna Ghadimi, Hamid Reza Feyzmahdavian, and Mikael Johansson. Global convergence of the heavy-ball method for convex optimization. In *2015 European control conference (ECC)*, pages 310–315. IEEE, 2015.

[18] Nicolas Flammarion and Francis Bach. From averaging to acceleration, there is only a step-size. In *Conference on Learning Theory*, pages 658–695. PMLR, 2015.

[19] Igor Gitman, Hunter Lang, Pengchuan Zhang, and Lin Xiao. Understanding the role of momentum in stochastic gradient methods. In H. Wallach, H. Larochelle, A. Beygelzimer, F. d Alché-Buc, E. Fox, and R. Garnett, editors, *Advances in Neural Information Processing Systems*, volume 32, pages 9633–9643. Curran Associates, Inc., 2019.

[20] Tao Sun, Penghang Yin, Dongsheng Li, Chun Huang, Lei Guan, and Hao Jiang. Non-ergodic convergence analysis of heavy-ball algorithms. In *Proceedings of the AAAI Conference on Artificial Intelligence*, volume 33, pages 5033–5040, 2019.

[21] Nicolas Loizou and Peter Richtárik. Momentum and stochastic momentum for stochastic gradient, newton, proximal point and subspace descent methods. *Computational Optimization and Applications*, 77(3):653–710, 2020.

[22] Tianbao Yang, Qihang Lin, and Zhe Li. Unified convergence analysis of stochastic momentum methods for convex and non-convex optimization. *arXiv preprint arXiv:1604.03257*, 2016.

[23] Sébastien Gadat, Fabien Panloup, Sofiane Saadane, et al. Stochastic heavy ball. *Electronic Journal of Statistics*, 12(1):461–529, 2018.

[24] Jun-Kun Wang and Jacob Abernethy. Quickly finding a benign region via heavy ball momentum in non-convex optimization. *arXiv preprint arXiv:2010.01449*, 2020.

[25] Damien Scieur and Fabian Pedregosa. Universal average-case optimality of polyak momentum. In Hal Daumé III and Aarti Singh, editors, *Proceedings of the 37th International Conference on Machine Learning*, volume 119 of *Proceedings of Machine Learning Research*, pages 8565–8572. PMLR, 13–18 Jul 2020.

[26] Alain Barrat, Silvio Franz, and Giorgio Parisi. Temperature evolution and bifurcations of metastable states in mean-field spin glasses, with connections with structural glasses. *Journal of Physics A: Mathematical and General*, 30(16):5593–5612, aug 1997.

[27] Giampaolo Folena, Silvio Franz, and Federico Ricci-Tersenghi. Rethinking mean-field glassy dynamics and its relation with the energy landscape: The surprising case of the spherical mixed p-spin model. *Physical Review X*, 10(3):031045, 2020.

[28] Emile Richard and Andrea Montanari. A statistical model for tensor pca. In Z. Ghahramani, M. Welling, C. Cortes, N. Lawrence, and K. Q. Weinberger, editors, *Advances in Neural Information Processing Systems*, volume 27, pages 2897–2905. Curran Associates, Inc., 2014.

[29] Stefano Sarao Mannelli, Giulio Biroli, Chiara Cammarota, Florent Krzakala, Pierfrancesco Urbani, and Lenka Zdeborová. Marvels and pitfalls of the langevin algorithm in noisy high-dimensional inference. *Physical Review X*, 10(1):011057, 2020.

[30] Paul Cecil Martin, ED Siggia, and HA Rose. Statistical dynamics of classical systems. *Physical Review A*, 8(1):423, 1973.

[31] C De Dominicis. Dynamics as a substitute for replicas in systems with quenched random impurities. *Physical Review B*, 18(9):4913, 1978.

[32] Andrea Crisanti and H-J Sommers. The sphericalp-spin interaction spin glass model: the statics. *Zeitschrift für Physik B Condensed Matter*, 87(3):341–354, 1992.

[33] Stefano Sarao Mannelli, Florent Krzakala, Pierfrancesco Urbani, and Lenka Zdeborová. Passed & spurious: Descent algorithms and local minima in spiked matrix-tensor models. In *International Conference on Machine Learning*, pages 4333–4342, 2019.

[34] Stefano Sarao Mannelli, Giulio Biroli, Chiara Cammarota, Florent Krzakala, and Lenka Zdeborová. Who is afraid of big bad minima? analysis of gradient-flow in spiked matrix-tensor models. In *Advances in Neural Information Processing Systems*, pages 8679–8689, 2019.

[35] Stefano Sarao Mannelli, Giulio Biroli, Chiara Cammarota, Florent Krzakala, Pierfrancesco Urbani, and Lenka Zdeborová. Complex dynamics in simple neural networks: Understanding gradient flow in phase retrieval. In H. Larochelle, M. Ranzato, R. Hadsell, M. F. Balcan, and H. Lin, editors, *Advances in Neural Information Processing Systems*, volume 33, pages 3265–3274. Curran Associates, Inc., 2020.

[36] Leticia F Cugliandolo and Jorge Kurchan. Analytical solution of the off-equilibrium dynamics of a long-range spin-glass model. *Physical Review Letters*, 71(1):173, 1993.

[37] Andrea Crisanti, Heinz Horner, and H-J Sommers. The sphericalp-spin interaction spin-glass model. *Zeitschrift für Physik B Condensed Matter*, 92(2):257–271, 1993.

[38] Andrea Crisanti and Luca Leuzzi. Spherical 2+ p spin-glass model: An analytically solvable model with a glass-to-glass transition. *Physical Review B*, 73(1):014412, 2006.

[39] Antonio Auffinger, Gérard Ben Arous, and Jiří Černỳ. Random matrices and complexity of spin glasses. *Communications on Pure and Applied Mathematics*, 66(2):165–201, 2013.

[40] Giampaolo Folena, Silvio Franz, and Federico Ricci-Tersenghi. Gradient descent dynamics in the mixed p-spin spherical model: finite-size simulations and comparison with mean-field integration. *Journal of Statistical Mechanics: Theory and Experiment*, 2021(3):033302, 2021.

[41] Guilhem Semerjian, Leticia F Cugliandolo, and Andrea Montanari. On the stochastic dynamics of disordered spin models. *Journal of statistical physics*, 115(1):493–530, 2004.

[42] Florent Krzakala and Lenka Zdeborová. Performance of simulated annealing in p-spin glasses. In *Journal of Physics: Conference Series*, volume 473, page 012022. IOP Publishing, 2013.

[43] Marc Mézard, Giorgio Parisi, and Miguel Angel Virasoro. *Spin glass theory and beyond: An Introduction to the Replica Method and Its Applications*, volume 9. World Scientific Publishing Company, 1987.

[44] Gérard Ben Arous, Amir Dembo, and Alice Guionnet. Cugliandolo-Kurchan equations for dynamics of spin-glasses. *Probability theory and related fields*, 136(4):619–660, 2006.

[45] Amir Dembo and Eliran Subag. Dynamics for spherical spin glasses: disorder dependent initial conditions. *Journal of Statistical Physics*, pages 1–50, 2020.

[46] Francesca Mignacco, Florent Krzakala, Pierfrancesco Urbani, and Lenka Zdeborová. Dynamical mean-field theory for stochastic gradient descent in gaussian mixture classification. In *2020 Conference on Neural Information Processing Systems-NeurIPS 2020*, 2020.

[47] Haim Sompolinsky, Andrea Crisanti, and Hans-Jurgen Sommers. Chaos in random neural networks. *Physical review letters*, 61(3):259, 1988.

[48] Francesca Mastrogiuseppe and Srdjan Ostojic. Intrinsically-generated fluctuating activity in excitatory-inhibitory networks. *PLoS computational biology*, 13(4):e1005498, 2017.

[49] Tankut Can, Kamesh Krishnamurthy, and David J Schwab. Gating creates slow modes and controls phase-space complexity in grus and lstms. In *Mathematical and Scientific Machine Learning*, pages 476–511. PMLR, 2020.

[50] Weijie Su, Stephen Boyd, and Emmanuel Candes. A differential equation for modeling nesterov's accelerated gradient method: Theory and insights. *Advances in neural information processing systems*, 27:2510–2518, 2014.

[51] Ning Qian. On the momentum term in gradient descent learning algorithms. *Neural networks*, 12(1):145–151, 1999.

[52] Leticia F Cugliandolo, Gustavo S Lozano, and Emilio N Nessi. Non equilibrium dynamics of isolated disordered systems: the classical hamiltonian p-spin model. *Journal of Statistical Mechanics: Theory and Experiment*, 2017(8):083301, 2017.

[53] Francesca Mignacco, Pierfrancesco Urbani, and Lenka Zdeborová. Stochasticity helps to navigate rough landscapes: comparing gradient-descent-based algorithms in the phase retrieval problem. *Machine Learning: Science and Technology*, 2021.

[54] Tommaso Castellani and Andrea Cavagna. Spin-glass theory for pedestrians. *Journal of Statistical Mechanics: Theory and Experiment*, 2005(05):P05012, 2005.

[55] Elisabeth Agoritsas, Giulio Biroli, Pierfrancesco Urbani, and Francesco Zamponi. Out-of-equilibrium dynamical mean-field equations for the perceptron model. *Journal of Physics A: Mathematical and Theoretical*, 51(8):085002, 2018.

1. For all authors...
   (a) Do the main claims made in the abstract and introduction accurately reflect the paper's contributions and scope? [Yes]
   (b) Did you describe the limitations of your work? [Yes]
   (c) Did you discuss any potential negative societal impacts of your work? [Yes] Refer to the conclusion and broader impact section.
   (d) Have you read the ethics review guidelines and ensured that your paper conforms to them? [Yes]

2. If you are including theoretical results...
   (a) Did you state the full set of assumptions of all theoretical results? [Yes] Refer to sections "model definition".
   (b) Did you include complete proofs of all theoretical results? [N/A] Our results are not rigorous but are consistently checked against numerical simulations. We comment on possible strategies to make them rigorous.

3. If you ran experiments...
   (a) Did you include the code, data, and instructions needed to reproduce the main experimental results (either in the supplemental material or as a URL)? [No] We use standard algorithms and provide details on the parameters. They can be easily reproduce in any computer.
   (b) Did you specify all the training details (e.g., data splits, hyperparameters, how they were chosen)? [Yes] All the figures resulting from the experiments contain details to reproduce them.
   (c) Did you report error bars (e.g., with respect to the random seed after running experiments multiple times)? [Yes]
   (d) Did you include the total amount of compute and the type of resources used (e.g., type of GPUs, internal cluster, or cloud provider)? [No] Tha data for each figure can be obtained in maximum one day of laptop simulation.

4. If you are using existing assets (e.g., code, data, models) or curating/releasing new assets...
   (a) If your work uses existing assets, did you cite the creators? [N/A]
   (b) Did you mention the license of the assets? [N/A]
   (c) Did you include any new assets either in the supplemental material or as a URL? [No]
   (d) Did you discuss whether and how consent was obtained from people whose data you're using/curating? [N/A]
   (e) Did you discuss whether the data you are using/curating contains personally identifiable information or offensive content? [N/A]

5. If you used crowdsourcing or conducted research with human subjects...
   (a) Did you include the full text of instructions given to participants and screenshots, if applicable? [N/A]
   (b) Did you describe any potential participant risks, with links to Institutional Review Board (IRB) approvals, if applicable? [N/A]
   (c) Did you include the estimated hourly wage paid to participants and the total amount spent on participant compensation? [N/A]

Supplemental Material

A Spiked matrix-tensor model

In this section we discuss how the DMFT equations of the spiked matrix-tensor model differ from the mixed p-spin model. The main difference is that the hidden solution deforms locally the loss function

$$
\begin{aligned}
\mathcal{H} = &-\frac{1}{\Delta_p}\sqrt{\frac{(p-1)!}{N^{p-1}}} \sum_{i_1,\dots,i_p=1}^{N} T_{i_1,\dots,i_p} x_{i_1}\dots x_{i_p} - \frac{1}{\Delta_2}\frac{1}{\sqrt{N}}\sum_{i,j=1}^{N} Y_{ij}x_i x_j + \\
&-\frac{1}{p\Delta_p}\left(\frac{1}{N}\sum_j x_j x_j^*\right)^p - \frac{1}{2\Delta_2}\left(\frac{1}{N}\sum_j x_j x_j^*\right)^2 + \frac{\mu}{4N}\left(\sum_{i=1}^{N} x_i^2 - N\right)^2.
\end{aligned}
\tag{39}
$$

As it clearly appears from the equation of the loss, the overlap of the hidden solution with the estimator plays an important role. This leads to two additional order parameters $m_x[t] = \frac{1}{N}\sum_j x_j[t]x_j^*$ and $m_y[t] = \frac{1}{N}\sum_j y_j[t]x_j^*$ (or $m_v(t) = \frac{1}{N}\sum_j v_j(t)x_j^*$ for massive gradient flow).

Since the stochastic part of the loss is unchanged, the derivation follows same steps shown in section 4 of the main text. They lead to modified dynamical equations where overlap with the hidden solution is present, for instance in Nesterov they are

$$
\begin{aligned}
x_0[t+1] = &\, y_0[t] + \alpha\Xi[t] - \alpha\mu\left(C_y[t,t]-1\right)y_0[t] + \\
&+\alpha^2\sum_{t''=0}^{t} R_y[t,t'']Q''\left(C_y[t,t'']\right)y_0[t''] + Q'(m_y[t])\boldsymbol{x}^*,
\end{aligned}
\tag{40}
$$

$$
y_0[t+1] = x_0[t+1] + \frac{t}{t+3}\left(x_0[t+1] - x_0[t]\right).
\tag{41}
$$

Finally, substituting the effective dynamics into the definition of the order parameters we obtain:

- **for Nesterov acceleration**

$$
\begin{aligned}
C_x[t+1,t'] = &\, C_{xy}[t,t'] + \alpha^2\sum_{t''=0}^{t'} R_x[t',t'']Q'\left(C_y[t,t'']\right) + \alpha^2\sum_{t''=0}^{t} R_y[t,t'']Q''\left(C_y[t,t'']\right)C_{xy}[t',t''] + \\
&-\alpha\mu\left(C_y[t,t]-1\right)C_y[t,t'] - Q'(m_y[t])m_x[t'],
\end{aligned}
$$

$$
\begin{aligned}
C_{xy}[t+1,t'] = &\, C_y[t,t'] + \alpha^2\sum_{t''=0}^{t'} R_y[t',t'']Q'\left(C_y[t,t'']\right) + \alpha^2\sum_{t''=0}^{t} R_y[t,t'']Q''\left(C_y[t,t'']\right)C_y[t',t''] + \\
&-\alpha\mu\left(C_y[t,t]-1\right)C_{xy}[t,t'] - Q'(m_y[t])m_y[t'],
\end{aligned}
$$

$$
C_{xy}[t',t+1] = C_x[t+1,t'] + \frac{t}{t+3}\left(C_x[t+1,t'] - C_x[t,t']\right),
$$

$$
C_y[t',t+1] = C_{xy}[t+1,t'] + \frac{t}{t+3}\left(C_{xy}[t+1,t'] - C_{xy}[t,t']\right),
$$

$$
R_x[t+1,t'] = R_y[t,t'] + \delta_{t,t'} + \alpha^2\sum_{t''=t'}^{t} R_y[t,t'']R_y[t'',t']Q''\left(C_y[t,t'']\right) - \alpha\mu\left(C_y[t,t]-1\right)R_y[t,t'],
$$

14

$$R_y[t', t+1] = R_x[t+1, t'] + \frac{t}{t+3}\left(R_x[t+1, t'] - R_x[t, t']\right),$$

$$m_x[t+1] = m_y[t] - \alpha\mu\left(C_y[t,t] - 1\right)m_y[t] + \alpha^2 \sum_{t''=0}^{t} R_y[t, t'']Q''\left(C_y[t, t'']\right)m_y[t''] + Q'\left(m_y[t]\right),$$

$$m_y[t+1] = m_x[t+1] + \frac{t}{t+3}\left(m_x[t+1] - m_x[t]\right),$$

with initial conditions $C_x[0,0] = 1$, $C_y[0,0] = 1$, $C_{xy}[0,0] = 1$, $R_x[t+1, t] = 1$, $R_y[t+1, t] = \frac{2t+3}{t+3}$, $m_x[0] = 0^+$, $m_y[0] = 0^+$;

- **for heavy ball momentum.**

$$C_y[t+1, t'] = \beta C_y[t, t'] + \mu\left(C_x[t, t] - 1\right)C_{xy}[t, t'] + \alpha \sum_{t''=0}^{t'} R_y[t', t'']Q'\left(C_x[t, t'']\right)$$

$$+ \alpha \sum_{t''=0}^{t} R_x[t, t'']Q''\left(C_x[t, t'']\right)C_{xy}[t'', t'] - Q'(m_x[t])m_y[t'];$$

$$C_{xy}[t', t+1] = \beta C_{xy}[t', t] + \mu\left(C_x[t, t] - 1\right)C_x[t, t'] + \alpha \sum_{t''=0}^{t'} R_x[t', t'']Q'\left(C_x[t, t'']\right)$$

$$+ \alpha \sum_{t''=0}^{t} R_x[t, t'']Q''\left(C_x[t, t'']\right)C_x[t', t''] - Q'(m_x[t])m_x[t'];$$

$$C_{xy}[t+1, t'] = C_{xy}[t, t'] - \alpha C_y[t+1, t'];$$

$$C_x[t+1, t'] = C_x[t, t'] - \alpha C_{xy}[t', t+1];$$

$$R_y[t+1, t'] = \beta R_y[t, t'] + \frac{1}{\alpha}\delta_{t,t'} + \mu\left(C_x[t, t] - 1\right)R_x[t, t']$$

$$+ \alpha \sum_{t''=0}^{t} R_x[t, t'']R_x[t'', t']Q''\left(C_x[t, t'']\right);$$

$$R_x[t+1, t'] = R_x[t, t'] - \alpha R_y[t+1, t']$$

$$m_y[t+1] = \beta m_y[t] - \mu\left(C_x[t, t] - 1\right)m_x[t] +$$

$$+ \sum_{t''=0}^{t} R_x[t, t'']Q''\left(C_x[t, t'']\right)m_x[t''] - Q'\left(m_x[t]\right),$$

$$m_x[t+1] = m_x[t] - \alpha m_y[t+1].$$

with initial conditions: $C_x[0,0] = 1$, $C_y[0,0] = 0$, $C_{xy}[0,0] = 0$, $R_y[t+1, t] = 1/\alpha$, $R_x[t+1, t] = -1$, $m_y[0] = O^+$, $m_x[0] = O^+$.

- **for massive gradient flow** (see Sec. C)

$$\partial_t C_x(t, t') = C_{xv}(t', t),$$

$$m\partial_t C_v(t, t') = -C_v(t, t') + \int_0^t dt'' R_{x|v}(t, t'')Q''[C_x(t, t'')]C_{xv}(t'', t') +$$

$$+ \int_0^{t'} Q'[C_x(t, t'')]R_v(t', t'') - \mu C_x(t.t')\left(C_x(t, t) - 1\right) + Q'[m_x(t')]m_x(t),$$

$$\partial_t C_{xv}(t, t') = C_v(t, t'),$$

$$m\partial_{t'} C_{xv}(t, t') = -C_{xv}(t, t') + \int_0^{t'} dt'' R_{x|v}(t', t'')Q''[C_x(t', t'')]C_x(t, t'') +$$

$$+ \int_0^t Q'[C_x(t', t'')]R_{x|v}(t, t'') - \mu C_{xv}(t, t')\left(C_x(t, t) - 1\right) + Q'[m_x(t)]m_v(t'),$$

$$m\partial_t R_v(t,t') = \delta(t-t') - R_v(t,t') + \int_{t'}^t dt'' Q''[C(t,t'')]R_{x|v}(t,t'')R_{x|v}(t'',t') +$$
$$- \mu R_{x|v}(t,t')\left(C_x(t,t)-1\right),$$
$$\partial_t R_{x|v}(t,t') = R_v(t,t'),$$
$$\partial_t m_x(t) = m_v(t),$$
$$m\partial_t m_v(t) = -m_v(t) + \int_0^t dt'' R_{x|v}(t,t'')Q''[C_x(t,t'')]m_x(t'') + Q'[m_x(t)] +$$
$$- \mu m_x(t)\left(C_x(t,t)-1\right),$$

with initial conditions are : $C_x(0,0) = 1$; $C_v(0,0) = 0$; $C_{xv}(0,0) = 0$; $R_v(t^+,t) = 1/m$; $R_{x|v}(t,t) = 0$; $m_x(0) = 0^+$. $m_y(0) = 0^+$.

Finally the equation to compute the loss in time is

$$\mathcal{L}[t] = -\frac{\alpha}{\Delta_p C_x[t,t]^{\frac{p}{2}}}\sum_{t''=0}^t R_x[t,t']C_x[t,t']^{p-1} - \frac{\alpha}{\Delta_2 C_x[t,t]}\sum_{t''=0}^t R_x[t,t']C_x[t,t'] - Q\left(m_x[t]\right). \tag{42}$$
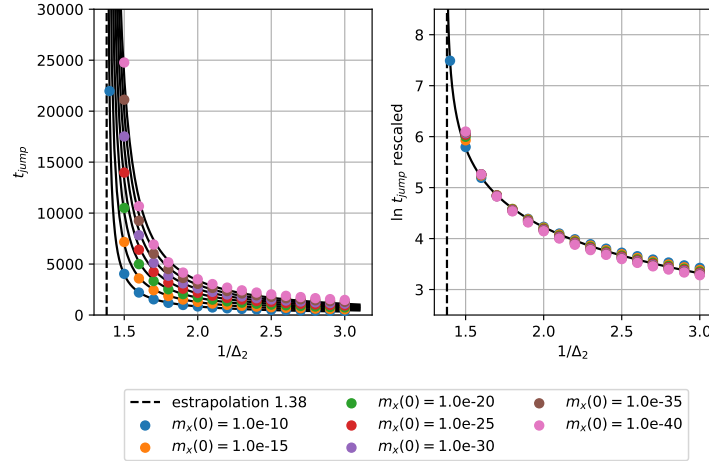
B Extracting the recovery threshold

Figure 5: **Algorithmic threshold extrapolated using Nesterov acceleration.** The dots are the divergence time obtained for the different values of Δ_2 with $\Delta_3 = 4.0$ fixed. On the right panel we show that these lines collapse to a single line once rescaled by a factor $a^{\ln m_x[0]}$ with $a \approx 1.089$.

The extrapolation procedure for $\Delta_3 = 4.0$ is shown in Fig. 5. The threshold obtained by fitting with a power law and observing the divergent Δ_2. On the left panel we plot the number of iteration before the algorithm jumps to the solution t_{jump} as a function of the signal to noise ratio $1/\Delta_2$. The figure also show remarkable effects of the initial conditions for m_x and m_y. These effects where already described and understood in [33].

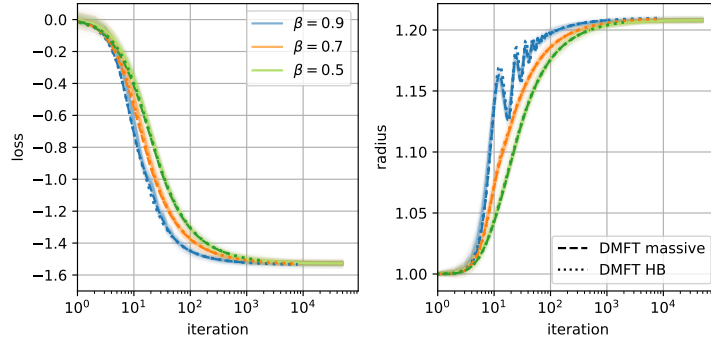16

C Correspondence with continuous HB equations

Figure 6: **Comparison of HB and massive with mapping.** The figure reproduce the same setting of Fig. 2 with the additional dashed line for the DMFT of massive gradient flow using the mapping.

An alternative way to analyze the HB dynamics is by using the results of [51] to map it to the massive momentum described by the flow equation

$$m\ddot{x}_i(t) + \dot{x}_i(t) = -\frac{\delta\mathcal{L}[\boldsymbol{x}(t)]}{\delta x_i(t)}. \tag{43}$$

The natural discretization of this equation is

$$\frac{m}{h^2}\left(x[k+1] - 2x[k] - x[k-1]\right) + \frac{1}{h}\left(x[k+1] - x[k]\right) = -\nabla\mathcal{L}(x[k]) \tag{44}$$

being h the time discretization step (analogous to the learning rate in gradient descent). Using the mapping of [51] we can identify

$$m = \frac{\beta\alpha}{(1-\beta)^2} \tag{45}$$

$$h = \frac{\alpha}{1-\beta} \tag{46}$$

Observe that in order to be consistent with a continuous dynamics we need the following scaling $\beta = \mathcal{O}(1)$, $\alpha = \mathcal{O}[(1-\beta)^2]$. We empirically observe in the simulations a good agreement between massive and HB even for $\beta = 0.999$ and $\alpha = 0.01$. In the following, when discussing the comparison between simulation and DMFT, we mean that we run HB algorithm and superimpose on its massive momentum description.

The massive momentum dynamics was also considered in [52] without the damping term ($\dot{x}_i(t)$) and for the model with a hard spherical constraint $\sum_i x_i[t]^2 = N$. While the DMFT derived in [52] completely describe the aforementioned particular case, the way in which it is written uses the fact that without damping the dynamics is conservative and the spherical constraint can be enforced using that. In our case we are not in this regime and therefore we resort to a different computation, that will lead us to quite different equations. Indeed if one wants to transform massive momentum in a practical algorithm one needs to transform the second order ODEs into first order by defining velocity variables $v_i(t) = \dot{x}_i(t)$. Then the discrete version of Eq. (43) is

$$x_i[t+1] = x_i[t] + hv_i[t]$$
$$v_i[t+1] = v_i[t] - \frac{h}{m}\,v_i[t] - \frac{h}{m}\,\frac{\delta\mathcal{H}}{\delta x_i[t]} \tag{47}$$

Analysing these equations through DMFT one gets a set of flow equations for the following dynamical order parameters $C_x[t,t'] = \sum_i x_i[t]x_i[t']/N$, $C_v[t,t'] = \sum_i v_i[t]v_i[t']/N$, $C_{xv}[t,t'] = \sum_i x_i[t]v_i[t']/N$, $R_v[t,t'] = \frac{1}{N}\sum_i \frac{\delta v_i[t]}{\delta H_i[t']}$, and $R_{x|v}[t,t'] = \frac{1}{N}\sum_i \frac{\delta x_i[t]}{\delta H_i[t']}$; where $\boldsymbol{H}$ is an instantaneous perturbation acting on the velocity. The result of the computation gives:

$$C_x[t+1,t'] = C_x[t,t'] + h\,C_{xv}(t',t)\ ; \tag{48}$$

17

$$C_v[t+1,t'] = C_v[t,t'] - \frac{h}{m} C_v(t,t') - \mu \frac{h}{m} C_{xv}(t,t') (C_x(t,t) - 1)$$
$$+ \frac{h^2}{m} \sum_{t''=0}^{t} R_{x|v}[t,t'']Q''(C_x[t,t'']) C_{xv}[t'',t'] + \frac{h^2}{m} \sum_{t''=0}^{t'} Q'(C_x[t,t'']) R_v[t',t''];$$

(49)

$$C_{xv}[t+1,t'] = C_{xv}[t,t'] + h\, C_v[t,t'];$$

(50)

$$C_{xv}[t,t'+1] = C_{xv}[t,t'] - \frac{h}{m} C_{xv}[t,t'] - \mu \frac{h}{m} C_x[t,t'] (C_x[t',t'] - 1)$$
$$+ \frac{h^2}{m} \sum_{t''=0}^{t'} R_{x|v}[t',t'']Q''(C_x[t',t'']) C_x[t,t''] + \frac{h^2}{m} \sum_{t''=0}^{t} Q'(C_x[t',t'']) R_{x|v}[t,t'']$$

(51)

$$R_v[t+1,t'] = R_v[t,t'] + \frac{h}{m} \delta_{t,t'} - \mu \frac{h}{m} R_{x|v}[t,t'] (C_x(t,t) - 1) - \frac{h}{m} R_v[t,t']$$
$$+ \frac{h^2}{m} \sum_{t''=0}^{t} Q''(C[t,t'']) R_{x|v}[t,t'']R_{x|v}[t'',t']$$

(52)

$$R_{x|v}[t+1,t'] = R_{x|v}[t,t'] + h\, R_v[t,t'].$$

(53)

and initial conditions : $C_x[0,0] = 1, C_v[0,0] = 0, C_{xv}[0,0] = 0, R_v[t+1,t] = 1/m, R_{x|v}[t+1,t] = 0$.
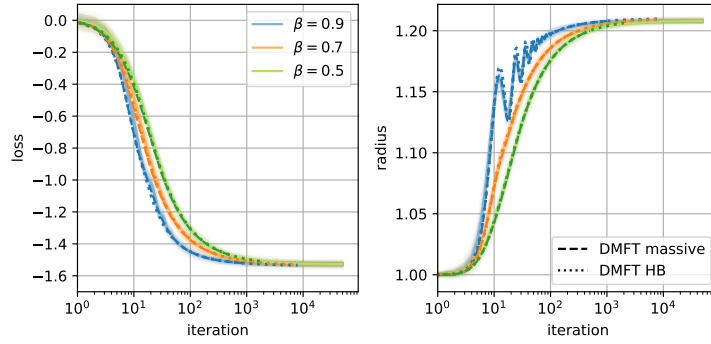

Figure 7: **Comparison of HB and with DMFT.** Simulations of HB momentum in the mixed p-spin model with $p = 3$, $\Delta_3 = 2/p$, $\Delta_2 = 1$, ridge parameter $\mu = 10$ and input dimension $N = 1024$. The parameters are $\alpha = 0.01$ for all the simulations and $\beta \in \{0.5, 0.7, 0.9, 0.99, 0.999\}$. We use solid line to represent the result from the simulation, the dotted line for the DMFT of massive gradient flow with the mapping. We empirically observe that in this problem the value of β that gives the best speed up is $\beta = 0.9$. In order the integrate the DMFT of massive gradient we matched the mass as described in Eq. (45) and consider time steps $h \in \{0.005, 0.005, 0.0125, 0.25, 0.25\}$.

Derivation of the DMFT equations for massive gradient flow In this section we derive the dynamical mean field theory (DMFT) equations of massive gradient flow in the mixed p-spin.

We use the generating functional approach described in [54, 55] to obtain the effective dynamical equations. First we rewrite de massive dynamics Eq. (43) as two ODEs

$$m\dot{\boldsymbol{v}}(t) = -\boldsymbol{v}(t) - \nabla\mathcal{H}[\boldsymbol{x}(t)],$$

(54)

$$\dot{\boldsymbol{x}}(t) = \boldsymbol{v}(t).$$

(55)

We use the following simple identity that takes the name of *generating functional*

$$1 = \mathcal{Z} = \int \mathcal{D}[\boldsymbol{x}, \boldsymbol{v}]\, \delta\left(m\dot{\boldsymbol{v}}(t) + \boldsymbol{v}(t) + \nabla\mathcal{H}[\boldsymbol{x}(t)]\right)\, \delta\left(\dot{\boldsymbol{x}}(t) - \boldsymbol{v}(t)\right)$$

(56)

$$= \int \mathcal{D}[\boldsymbol{x}, \tilde{\boldsymbol{x}}, \boldsymbol{v}, \tilde{\boldsymbol{v}}] \prod_{i=1}^{N} \exp\left\{i \int \tilde{v}_i(t) \left[m\dot{v}_i(t) + v_i(t) + \nabla_i\mathcal{H}[\boldsymbol{x}(t)]\right] dt\right\} \exp\left\{i \int \tilde{x}_i(t) \left[\dot{x}_i(t) - v_i(t)\right] dt\right\}$$

(57)

where in the first line we integrate over all possible trajectories of $\boldsymbol{v}$ and $\boldsymbol{x}$, and we impose them to match the massive gradient flow equations using Dirac's deltas. In the second line we use the Fourier representation of the delta and we absorb the normalization constants in the term $\mathcal{D}[\boldsymbol{x}, \tilde{\boldsymbol{x}}, \boldsymbol{v}, \tilde{\boldsymbol{v}}]$. We can now average over the stochasticity of the problem, let us indicate with an overline the average.

$$1 = \overline{\mathcal{Z}} = \int \mathcal{D}[\boldsymbol{x}, \tilde{\boldsymbol{x}}, \boldsymbol{v}, \tilde{\boldsymbol{v}}] \prod_{i=1}^{N} \exp\left\{ i \int \tilde{v}_i(t) \left[m\dot{v}_i(t) + v_i(t) \right] dt \right\} \exp\left\{ i \int \tilde{x}_i(t) \left[\dot{x}_i(t) - v_i(t) \right] dt \right\} \times \tag{58}$$

$$\overline{\times \prod_{i=1}^{N} \exp\left\{ i \int \tilde{v}_i(t) \left[\sqrt{\frac{(p-1)!}{N^{p-1}}} \sum_{(i,i_2,\dots,i_p)} \xi^{(p)}_{i,i_2,\dots,i_p} x_{i_2}(t) \dots x_{i_p}(t) + \frac{1}{\sqrt{N}} \sum_j \xi^{(2)}_{i,j} x_j(t) \right] dt \right\} \times} \tag{59}$$

$$\times \prod_{i=1}^{N} \exp\left\{ i \int \tilde{v}_i(t) \mu \left(\frac{1}{N} \sum_j x_j^2(t) - 1 \right) x_i(t) dt \right\} \tag{60}$$

We can proceed integrating the second line over the noise. Importantly we must group all the element that multiply a given $\xi^{(p)}$. Considering only second line and neglecting constant multiplicative factors we obtain

$$\exp\left\{ -\frac{N}{2p\Delta_p} \int \left[p \left(\sum_i \frac{\tilde{v}_i(t)\tilde{v}_i(t')}{N} \right) \left(\sum_i \frac{x_i(t)x_i(t')}{N} \right)^{p-1} + \right.\right.$$

$$\left.\left. + p(p-1) \left(\sum_i \frac{\tilde{v}_i(t)x_i(t')}{N} \right) \left(\sum_i \frac{x_i(t)\tilde{v}_i(t')}{N} \right) \left(\sum_i \frac{x_i(t)x_i(t')}{N} \right)^{p-2} \right] dt' dt \right\} \times$$

$$\times \exp\left\{ -\frac{N}{2\Delta_2} \int \left[\left(\sum_i \frac{\tilde{v}_i(t)\tilde{v}_i(t')}{N} \right) \left(\sum_i \frac{x_i(t)x_i(t')}{N} \right) + \left(\sum_i \frac{\tilde{v}_i(t)x_i(t')}{N} \right) \left(\sum_i \frac{x_i(t)\tilde{v}_i(t')}{N} \right) \right] dt' dt \right\}$$

We define $Q(x) = x^p/(p\Delta_p) + x^2/(2\Delta_2)$ and the order parameters

$$C_x[t,t'] = \sum_i x_i[t]x_i[t']/N, \tag{61}$$

$$C_v[t,t'] = \sum_i v_i[t]v_i[t']/N, \tag{62}$$

$$C_{xv}[t,t'] = \sum_i x_i[t]v_i[t]/N, \tag{63}$$

$$R_v[t,t'] = \frac{1}{N} \sum_i \frac{\delta v_i[t]}{\delta H_i[t']}, \tag{64}$$

$$R_{x|v}[t,t'] = \frac{1}{N} \sum_i \frac{\delta x_i[t]}{\delta H_i[t']}; \tag{65}$$

and enforce some of them using Dirac's deltas

$$\int \mathcal{D}[C_x, C_{\tilde{v}}, C_{x\tilde{v}}, C_{\tilde{v}x}] \delta\left(NC_{\tilde{v}}(t,t') - \sum_j i\,\tilde{v}_j(t)\, i\,\tilde{v}_j(t') \right) \delta\left(NC_x(t,t') - \sum_j x_j(t)\, x_j(t') \right) \times$$

$$\times \delta\left(NC_{x\tilde{v}}(t,t') - \sum_j x_j(t)\, i\,\tilde{v}_j(t') \right) \delta\left(NC_{\tilde{v}x}(t,t') - \sum_j i\,\tilde{v}_j(t)\, x_j(t') \right) \times$$

$$\times \exp\left\{ -\frac{N}{2\Delta_p} \int \left[C_{\tilde{v}}(t,t')Q'\left[C_x(t,t')\right] + C_{\tilde{v}x}(t,t')C_{x\tilde{v}}(t,t')Q''\left[C_x(t,t')\right] \right] dt' dt \right\}.$$

19

Using again the Fourier representation of the deltas and considering N large, the auxiliary variables introduced with the transform concentrate to their saddle point according to Laplace approximation. Furthermore it is easy to show [54] that $C_{x\tilde{v}}(t, t') = C_{\tilde{v}x}(t', t)$ and $C_{x\tilde{v}}(t, t') = R_{x|v}(t, t')$, with $R_{x|v}$. Under this considerations, we rewrite the average generating functional

$$1 = \overline{\mathcal{Z}} = \int \mathcal{D}[\boldsymbol{x}, \tilde{\boldsymbol{x}}, \boldsymbol{v}, \tilde{\boldsymbol{v}}] \prod_{i=1}^{N} \exp\left\{ i \int \tilde{v}_i(t) \left[m\dot{v}_i(t) + v_i(t) + \mu \left(\frac{\sum_j x_j^2(t)}{N} - 1 \right) x_i(t) \right] dt \right\} \times$$

(66)

$$\times \prod_{i=1}^{N} \exp\left\{ i \int \tilde{x}_i(t) \left[\dot{x}_i(t) - v_i(t) \right] dt \right\} \times$$

(67)

$$\times \exp\left\{ -\int \sum_j \left[\frac{1}{2} Q'[C_x(t, t')] i\,\tilde{v}_j(t)\, i\,\tilde{v}_j(t') - Q''[C_x(t, t')] R_{x|v}(t, t')\, i\,\tilde{v}_j(t')\, x_j(t) \right] dt' dt \right\}.$$

(68)

Finally we can take a Hubbard-Stratonovich transform on the first term of the second line and identify a stochastic process $\Xi(t)$ with zero mean at all times and covariance $\mathbb{E}[\Xi(t)\Xi(t')] = Q'[C_x(t, t')]$. The resulting generating functional now represent the dynamics in $\boldsymbol{x}$ and $\boldsymbol{v}$ where the cross-element interactions are replaced by the stochastic process. The resulting effective equations are

$$m\dot{\boldsymbol{v}}(t) = -\boldsymbol{v}(t) + \int_0^t dt'' R_{x|v}(t, t'') Q'[C_x(t, t'')]\boldsymbol{x}(t'') + \boldsymbol{\Xi}(t) - \mu \left[C_x(t, t) - 1 \right] \boldsymbol{x}(t),$$

(69)

$$\dot{\boldsymbol{x}}(t) = \boldsymbol{v}(t).$$

(70)

Finally we introduce the order parameters Eqs. (61-65) and compute their equation explicitly by substituting the equations of the effective dynamics. In order to do that, we use Girsanov theorem and evaluate the following expected values

$$\langle v(t)\Xi(t') \rangle = \int_0^{t'} dt'' R_v(t, t'') Q'[C_x(t, t'')],$$

(71)

$$\langle x(t)\Xi(t') \rangle = \int_0^{t'} dt'' R_{x|v}(t, t'') Q'[C_x(t, t'')].$$

(72)

The dynamical equations are

$$\partial_t C_x(t, t') = C_{xv}(t', t);$$

(73)

$$m\partial_t C_v(t, t') = -C_v(t, t') + \int_0^t dt'' R_{x|v}(t, t'') Q''[C_x(t, t'')] C_{xv}(t'', t') +$$

$$+ \int_0^{t'} Q'[C_x(t, t'')] R_v(t', t'') - \mu C_x(t, t') \left(C_x(t, t') - 1 \right);$$

(74)

$$\partial_t C_{xv}(t, t') = C_v(t, t');$$

(75)

$$m\partial_{t'} C_{xv}(t, t') = -C_{xv}(t, t') + \int_0^{t'} dt'' R_{x|v}(t', t'') Q''[C_x(t', t'')] C_x(t, t'') +$$

$$+ \int_0^t Q'[C_x(t', t'')] R_{x|v}(t, t'') - \mu C_{xv}(t, t') \left(C_x(t, t') - 1 \right);$$

(76)

$$m\partial_t R_v(t, t') = \delta(t - t') - R_v(t, t') + \int_{t'}^t dt'' Q''[C(t, t'')] R_{x|v}(t, t'') R_{x|v}(t'', t') +$$

$$- \mu R_{x|v}(t, t') \left(C_x(t, t') - 1 \right);$$

(77)

$$\partial_t R_{x|v}(t, t') = R_v(t, t').$$

(78)

and $\mu(t) = C_{xv}(t, t)$.

The initial conditions are :

$$C_x(t, t) = 1 \; ; \tag{79}$$
$$C_v(t = 0, t = 0) = 0 \; ; \tag{80}$$
$$C_{xv}(t = 0, t = 0) = 0 \; ; \tag{81}$$
$$R_v(t^+, t^+) = 1/m \; ; \tag{82}$$
$$R_{x|v}(t, t) = 0 \; . \tag{83}$$

Where Eq. (79) comes from the spherical constraint; Eqs. (80,81) come from the initialization with no kinetic energy $\boldsymbol{v}(0) = \boldsymbol{0}$; Eqs. (82) and (83) come from Eqs. (69) and (70) (respectively) after deriving by $\Xi(t')$, integrating on t in $[t - h; t + h]$ (with $h \to 0$) and taking $t' \to t$. The equations shown in the main text are the discrete equivalent of the ones just obtained.

D   Hard spherical constraint

It is also possible to consider a hard spherical constraint, which is the situation typically considered in the physics literature [32, 36]. A massive dynamics was already considered in [52] but their derivation was in the underdamped regime where the total energy is conserved. Using that approach the conservation of the energy was key. Unfortunately the energy is not conserved in general, and in particular in the case of optimization where we aim to go down in energy in order to find a minimum.

For reference sake we consider massive gradient flow, the same considerations apply straightforwardly to Nesterov acceleration. Let us write the dynamics in this case splitting the system in two ODEs

$$m\dot{\boldsymbol{v}}(t) = -\boldsymbol{v}(t) - \nabla\mathcal{L}[\boldsymbol{x}(t)], \tag{84}$$
$$\dot{\boldsymbol{x}}(t) = \boldsymbol{v}(t) - \mu(t)\boldsymbol{x}(t). \tag{85}$$

The last term in the second line constraints the dynamics to move in the sphere by removing the terms of the velocity that move orthogonally to the sphere. Therefore the term $\mu(t)$ is given by the projection of the velocity in the direction that is tangent to the sphere $\sum_j x_j(t)v_j(t)/N$.

We can then follow the usual techniques, e.g. section C, and obtain

$$\partial_t C_x(t, t') = -\mu(t)C_x(t, t') + C_{xv}(t', t) \;, \tag{86}$$

$$m\partial_t C_v(t, t') = -C_v(t, t') + \int_0^t dt'' R_{x|v}(t, t'')Q''[C_x(t, t'')]C_{xv}(t'', t') + \int_0^{t'} Q'[C_x(t, t'')]R_v(t', t'') \;, \tag{87}$$

$$\partial_t C_{xv}(t, t') = -\mu(t)C_{xv}(t, t') + C_v(t, t') \;, \tag{88}$$

$$m\partial_{t'} C_{xv}(t, t') = -C_{xv}(t, t') + \int_0^{t'} dt'' R_{x|v}(t', t'')Q''[C_x(t', t'')]C_x(t, t'') + \int_0^t Q'[C_x(t', t'')]R_{x|v}(t, t'') \;, \tag{89}$$

$$m\partial_t R_v(t, t') = \delta(t - t') - R_v(t, t') + \int_{t'}^t dt'' Q''[C(t, t'')]R_{x|v}(t, t'')R_{x|v}(t'', t') \;, \tag{90}$$

$$\partial_t R_{x|v}(t, t') = -\mu(t)R_{x|v}(t, t') + R_v(t, t'); \tag{91}$$

with $\mu(t) = C_{xv}(t, t)$ and initial conditions $C_x(t, t) = 1$, $C_v(0, 0) = 0$, $C_{xv}(0, 0) = 0$, $R_v(t^+, t) = \frac{1}{m}$, $R_{x|v}(t, t) = 0$.